Dalton Transactions

The loading of PPy on surface of transition metal coordination polymer modified polyoxometalate (TMCP/POM): a feasible strategy to obtain visible light active and high quantum yields POM based photocatalyst

Journal:	*Dalton Transactions*
Manuscript ID:	DT-ART-04-2014-001279.R2
Article Type:	Paper
Date Submitted by the Author:	25-Jun-2014
Complete List of Authors:	xu, xinxin; Inorganic Institution, Chemistry Department Gao, Xin; Inorganic Institution, Chemistry Department Cui, Zhong-Ping; Inorganic Institution, Chemistry Department Liu, Xiaoxia; Inorganic Institution, Chemistry Department Zhang, Xia; Inorganic Institution, Chemistry Department

Graphical Abstract

The loading of PPy on surface of transition metal coordination polymer modified polyoxometalate (TMCP/POM): a feasible strategy to obtain visible light active and high quantum yields POM based photocatalyst

Xinxin Xu, Xin Gao, Zhongping Cui, Xiaoxia Liu* and Xia Zhang*

Department of Chemistry, College of Science, Northeast University, Shenyang, Liaoning, 110819, People's Republic of China

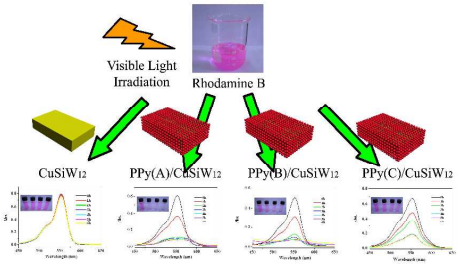

PPy loaded **TMCP/POM** composite materials were fabricated successfully, which displays more excellent photocatalytic activity than **TMCP/POM** under visible light irradiation.

The loading of PPy on surface of transition metal coordination polymer modified polyoxometalate (TMCP/POM): a feasible strategy to obtain visible light active and high quantum yields POM based photocatalyst

Xinxin Xu, Xin Gao, Zhongping Cui, Xiaoxia Liu* and Xia Zhang*

Department of Chemistry, College of Science, Northeast University, Shenyang, Liaoning, 110819, People's Republic of China

*Author to whom correspondence should be addressed.

Tel: +86-024-83689510, Fax: +86-024-23600159.

E-mail: xxliu@mail.neu.edu.cn (Professor X. X. Liu)

xzhang@ mail.neu.edu.cn (Professor X. Zhang)

Abstract

To improve photocatalytic activity of a transition metal coordination polymer modified polyoxometalate (**TMCP/POM**), polypyrrole (PPy) was loaded on its surface through a facile in-situ chemical oxidation polymerization process. Under the irradiation of visible light, PPy loaded **TMCP/POM** composite material exhibited more excellent photocatalytic activity than **TMCP/POM**, PPy and their mechanically blended products on degradation of Rhodamine B (RhB). Optical and electrochemical tests illustrated the enhancement of photocatalytic activity can be attributed to high separation efficiency of photogenerated electron-hole pair on the interface of PPy and **TMCP/POM**, which originates from synergy effect between them. Furthermore, the influence of reaction temperature on morphology, wettability, conductivity and photocatalytic performance of the resulting composite material were discussed and an optical temperature to fabricate photocatalyst with high efficiency had been obtained. These results suggest the loading of PPy on surface of **TMCP/POM** would be a feasible strategy to enhance its photocatalytic activity.

Introduction

Recently, organic dyes produced in textile industries have become the major sources in water contamination and photocatalytic degradation has been proved to be an efficient and economical way to decompose these pollutants into less dangerous matter.[1, 2] As a kind of green and cheap photocatalyst, which possesses similar valence band position and band gap (E_g) with TiO_2, **TMCP/POM** has been studied to remove organic dyes from water.[3] Compared with other polyoxometalate based photocatalysts, the solubility of **TMCP/POM** is much lower, which makes them more convenient in recovering and recycling.[4] Furthermore, as a low-price and nontoxicity photocatalyst, **TMCP/POM** also exhibits the advantages such as high photocatalytic efficiency and excellent chemical stability to decompose pollutants in water.[5] But the drawbacks such as inactive in visible light region and low quantum yields still impede further applications of **TMCP/POM** in waste water treatment. Now, the extension of photoresponse region and the enhancement of quantum yields become significant problems in the exploration of **TMCP/POM**.[6, 7]

To resolve these problems, the loading of a visible light active material, which possesses excellent photogenerated electron-hole pair separation property on surface of **TMCP/POM**, may be a feasible strategy. In this aspect, PPy is a suitable option, which meets all these requirements perfectly: firstly, PPy exhibits strong photoresponse in visible and ultraviolet light region; secondly, PPy is an excellent photogenerated hole transporting material, which can separate electron-hole pair effectively.[8] Furthermore, compared with other conducting polymers, such as polyaniline (PANI) and polythiophene (PT), the polymerization process of PPy is mild, which can not affect the stability of **TMCP/POM**.[9] Up to now, PPy has been employed to improve the photocatalytic activities of some oxide photocatalysts and

received very favorable results.[10-14] Inspired by these, we decide to improve the photocatalytic property of **TMCP/POM** through its combination with PPy.

Our imagination was confirmed to be reasonable by a series of visible light active photocatalysts, named **PPy/CuSiW$_{12}$**, which were synthesized by the loading of PPy on surface of a new **TMCP/POM**, $[Cu_4(pca)_2(bpca)_2(H_2O)_2(SiW_{12}O_{40})_2]\cdot(H_2O)_2]_n$ (**CuSiW$_{12}$**, pca = pyridine-2-carboxylic acid, bpca = bis(2-pyridylcarbonyl)amine). Photocatalytic degradation of RhB was investigated and results indicated the loading of PPy on surface of **CuSiW$_{12}$** enhanced its photocatalytic activity and quantum yields effectively. During polymerization of PPy, temperature has great effects on its chemical and physical properties, such as conductivity and morphology, which may further influence photocatalytic and wettability of the resulted **PPy/CuSiW$_{12}$** composite material. To make this point clear, in-situ chemical oxidative polymerization of pyrrole (Py) was conducted under different conditions and an optical temperature to achieve **PPy/CuSiW$_{12}$** composite material with excellent photocatalytic activity was obtained.

Experimental section

Materials and synthesis

All purchased chemicals were of reagent grade and used without further purification. The morphology was observed on an EVO18 field emission scanning electron microscope (ZEISS, Germany). PXRD patterns were recorded on D8 X-ray diffractometer, employing monochromatized Cu Kα incident radiation. FTIR spectra were recorded in the range 4000-400 cm^{-1} on an Alpha Centaur FTIR spectrophotometer using KBr pellets. Diffuse reflectance spectra (DRS) were recorded on a Shimadzu-2501PC spectrometer using $BaSO_4$ as a standard. The conductivity measurement was performed by conventional four-probe technique.

Electrochemical experiments were conducted on CHI 660B electrochemical workstation. The UV-visible adsorption spectrum was recorded using a Hitachi U-3010 UV-visible spectrometer. HPLC-MS was conducted by Agillent-1100, Bureher Esquier 3100t with YMC C-18 column.

Synthesis of $[Cu_4(pca)_2(bpca)_2(H_2O)_2(SiW_{12}O_{40})_2]\cdot(H_2O)_2]_n$ ($CuSiW_{12}$)

$CuSiW_{12}$ was prepared from the mixture of $Cu(NO_3)_2\cdot 3H_2O$ (0.024 g, 0.1 mmol), tpt (0.031 g, 0.1 mmol), $H_4SiW_{12}O_{40}$ (0.288 g, 0.1 mmol), and 10 mL H_2O. The mixture was stirred for 20 minutes and then transferred to a 23 mL Teflon-lined stainless steel bomb and kept at 180˚C under autogenously pressure for 4 days. The reaction system was cooled to room temperature during 24 hours. A large amount of block blue crystals of **$CuSiW_{12}$** were obtained. Yield: 55% (based on Cu).

Synthesis of PPy/$CuSiW_{12}$ composite materials

Py (0.034 g, 5 x 10^{-4} mol) was dissolved in 20 mL H_2O. **$CuSiW_{12}$** (3.875 g, 1 x 10^{-3} mol) was placed in above solution and dispersed with supersonic for 20 minutes. 10 ml $FeCl_3\cdot 6H_2O$ (0.05M) was slowly added to above mixture as oxidant. The product was stirred for 5 minutes and left undisturbed for 10 hours. The resulting **PPy/$CuSiW_{12}$** composite material was separated, rinsed with water, alcohol and finally dried at 60˚C for 24 hours in an oven. This experiment was conducted under different temperatures (A: 263K, B: 278K, C: 293K) and three **PPy/$CuSiW_{12}$** composite materials were prepared. The resulting products were referred to **PPy(A)/$CuSiW_{12}$**, **PPy(B)/$CuSiW_{12}$** and **PPy(C)/$CuSiW_{12}$** respectively. Before polymerization, the pH value of the reaction system is 7.2. After reaction, the pH values of these three systems are very close, which are 6.7, 6.5 and 6.8 respectively.

Synthesis of PPy and **PPy/$CuSiW_{12}$M**

PPy(A) to PPy(C) were obtained with a similar process with **PPy/$CuSiW_{12}$**

composite material, except **$CuSiW_{12}$** was not added. **PPy(A)/$CuSiW_{12}$M** to **PPy(C)/$CuSiW_{12}$M** were synthesized by the mixing of PPy and **$CuSiW_{12}$** with molar ratio of 1:3.

Wetting behavior test of PPy/$CuSiW_{12}$ composites materials

A droplet of the sample suspension in ethanol was placed on a cleaned glass substrate fixed on a spin coater at a rotating speed of 2000 rpm for 4 minutes, and a **PPy/$CuSiW_{12}$** film would be formed after drying. The wettability of the as-prepared films was characterized by measuring the water contact angle (CA) with a contact angle meter. A 2 μL water droplet was placed on this particle array film for water CA measurement. CA values were obtained by averaging three measurements on different areas of the sample surface.

Photocatalytic activity study

The photocatalytic activities of samples were evaluated by the degradation of RhB in the aqueous solution. 80 ml RhB aqueous solution with concentration of 10^{-5} M was mixed with 20 mg catalysts, which was exposed to illumination. Before turning on the lamp, the suspension containing RhB and photocatalyst were magnetically stirred in a dark condition for 40 min till an adsorption-desorption equilibrium was established. Samples were then taken out regularly from the reactor and centrifuged immediately for separation of any suspended solid. The transparent solution was analyzed by a UV-vis spectrometer. A 300 W medium pressure mercury lamp served as an ultraviolet light source and a 300 W Xe lamp with a cutoff filter ($\lambda \geq 420$ nm) served as a visible light source.

Electrochemical measurements

Photoelectrochemical tests were carried out with a conventional three-electrode system in quartz cell filled with 0.1 M Na_2SO_4 electrolyte (100 mL). The

$CuSiW_{12}$/ITO or **PPy/$CuSiW_{12}$/ITO** electrodes served as the working electrode. The counter and reference electrodes were a Pt plate and a saturated calomel electrode (SCE), respectively. A 300 W Xe lamp with a cutoff filter ($\lambda \geq 420$ nm) were used as the excitation light source for visible irradiation. For incident photonto-electron conversion efficiency (IPCE) measurements, a solution of 0.05 M I_2 and 0.5 M LiI in propylene carbonate was used as an electrolyte. The monochromatic light was from a 300 W Xe lamp, which was passed through a grating monochromator and the wavelength was selected at 5 nm intervals between 280 and 600 nm. Electrochemical impedance spectra (EIS) were recorded in potentiostatic mode. The amplitude of sinusoidal wave was 10 mV, and the frequency range of the sinusoidal wave was from 100 kHz to 0.05 Hz.

X-ray crystallography

Suitable single crystal of **$CuSiW_{12}$** was carefully selected under an optical microscope and glued on glass fibers. Structural measurements were performed on a Bruker AXS SMART APEX II CCD diffractometer at 293 K. The structures were solved by the direct method and refined by the full-matrix least-squares method on F^2 using the SHELXTL 97 crystallographic software package.[15] Anisotropic thermal parameters were used to refine all non-hydrogen atoms. Carbon-bound hydrogen atoms were placed in geometrically calculated positions; Oxygen-bound hydrogen atoms were located in the difference Fourier maps, kept in that position and refined with isotropic temperature factors. The X-ray structural analysis is given in Table S1. Further details of the crystal structure have been deposited to the Cambridge Crystallographic Data Centre as supplementary publication, which can be obtain free of charge (CCDC 994160). The Cambridge Crystallographic Data Centre via www.ccdc.cam.ac.uk/data_request/cif.

Structure, morphology and wettability study

Single crystal X-ray analysis reveals the fundamental unit of **$CuSiW_{12}$** is made up by one Keggin type polyanion $SiW_{12}O_{40}^{4-}$ (abbreviated as SiW_{12}), two Cu(II) cations (Cu1 and Cu2), one pca ligand and one bpca ligand (Fig. 1a). The Cu1 connects with three nitrogen atoms from bpca ligand, one oxygen atom from pca ligand and one oxygen atom form SiW_{12}. The Cu-N bond distances range from 1.909(17) to 2.029(17) Å and the Cu-O band distances are 1.990(15) and 2.441(14) Å respectively. This results a distorted pyramid coordination mode of Cu1. As Cu1, Cu2 also adopts five coordinated mode, which links with four oxygen atoms and one nitrogen atom. In these oxygen atoms, two come from bpca ligands, one comes from pca ligand and the last oxygen atom comes from coordinated water molecule. The Cu-O bond distances are in the range of 1.943(16) to 2.166(13) Å. The last coordination site of Cu2 is occupied by a nitrogen atom from pca ligand with Cu-N bond distance 1.952(16) Å. Such two Cu atoms are connected by bpca and pca ligands, which leads to a transition metal coordination polymer (**TMCP**), $[Cu_2(bpca)(pca)]_n$ (Fig. 1b). In **$CuSiW_{12}$**, the structure of SiW_{12} is similar with Keggin polyanion in other **TMCP/POMs**.[16,17] The central SiO_4 tetrahedron shares its oxygen atoms with four $\{W_3\}$ groups, which are linked to each other by corner-sharing mode. The Si-O band distances vary from 1.55(3) to 1.64(3) Å and O-Si-O band angles are in the range of 68.4(3) to 111.7(13)°. The W-O distances can be divided into three groups: The $W\text{-}O_t$ band distances range from 1.658(14) to 1.696(13) Å, $W\text{-}O_{b/c}$ band distances are in the range of 1.87(2) to 1.95(2) Å and $W\text{-}O_a$ band distances vary from 2.35(3) to 2.49(2) Å. Such SiW_{12} units are connected by $[Cu_2(bpca)(pca)]_n$ with Cu1-O20 = 2.442(17) Å and results the two-dimensional layer like structure of **$CuSiW_{12}$** (Fig. 1c). To our interests, at the beginning, tpt was added into the reaction system as reactant, but in the structure of

$CuSiW_{12}$, bpca and pca appeared. This should be ascribed to the catalysis function of Cu(II), which lead to the hydrolysis of tpt under hydrothermal condition (Fig. 1d). Although the hydrolysis of tpt has been studied by some researchers, such a "two birds with one stone" phenomenon has never been reported in the hydrolysis of tpt with the catalysis of Cu(II).[18] The thermogravimetric analysis (TGA) of **$CuSiW_{12}$** was carried out from 30 to 800°C (Fig. S1). The first weight loss in the temperature range of 91 to 148 °C is due to the loss of guest and coordinated water molecules. Over the range of 328 to 433°C, the weight loss should correspond to the decomposition of organic ligands.

The morphologies of **$CuSiW_{12}$** and **PPy/$CuSiW_{12}$** composite materials were studied with SEM. It can be observed clearly, **$CuSiW_{12}$** exhibits smooth surface and sharp fringe (Fig. 2a). **PPy/$CuSiW_{12}$** composite materials are significantly different from **$CuSiW_{12}$** due to the wrapping of PPy, which show coarse, irregular surface and circular fringe (Fig. 2b to 2d, inset). In high-magnification image, we can observe **PPy/$CuSiW_{12}$** composite materials more clearly and find temperature has great effects on their morphologies. As temperature is 263 K, **$CuSiW_{12}$** is coated by PPy particles with diameter about 60 to 80 nm (Fig. 2b). If temperature rises, we can find the dimensions of PPy particles grow slowly. When temperature is 278 K, the dimensions of PPy become 120 to 150 nm (Fig. 2c). If temperature rises continuously and reaches 293K, PPy particles with the size about 200 to 300 nm are found loading on surface of **$CuSiW_{12}$** (Fig. 2d).

The surface wettabilities of **$CuSiW_{12}$** and **PPy/$CuSiW_{12}$** were evaluated by contact angle (CA). For **$CuSiW_{12}$**, its CA value is 59.4 º, which is larger than **PPy/$CuSiW_{12}$** composite materials (Fig. 3a). This can be attributed to the differences in wettability between **$CuSiW_{12}$** and PPy, because PPy is more hydrophilic than **$CuSiW_{12}$**. As for

PPy/CuSiW$_{12}$, with the changing of temperature, their CA values are also in great difference. From **PPy(A)/CuSiW$_{12}$** to **PPy(C)/CuSiW$_{12}$**, their CA values are 36.4 º, 43.1 º and 49.7 º respectively (Fig. 3b to 3d). This lies in the diversities in morphology and size of PPy. Because smaller PPy particles often lead to smooth surface, while PPy with larger size usually results in coarse surface. So, in these composite materials, the CA value of **PPy(A)/CuSiW$_{12}$** is the smallest, while **PPy(C)/CuSiW$_{12}$** possesses the largest CA. This result indicates temperature is an important factor which has great effect on wettability of resulted **PPy/CuSiW$_{12}$** composite materials.

PXRD was applied to study the structure of composite materials (Fig. 4a). **PPy/CuSiW$_{12}$** composite materials exhibit similar diffraction patterns with **CuSiW$_{12}$**, which illustrates although $FeCl_3$ is used during polymerization of Py; the structure of **CuSiW$_{12}$** is still retained. Furthermore, the peaks belong to PPy are not observed, which illustrates the content of PPy may be too small to determine its existence. In the composite materials, to study the interactions between **CuSiW$_{12}$** and PPy, FTIR spectra were employed (Fig. 4b). In **PPy/CuSiW$_{12}$**, the characteristic bands at 781, 923 and 973 cm^{-1} can be attributed to the stretching of W=O, W-O and Si-O respectively, while the peaks appear at 3250 to 3400 cm^{-1} can be attributed to N-H stretching of PPy. Compared with pure **CuSiW$_{12}$** and PPy, in **PPy/CuSiW$_{12}$**, the W=O and W-O stretching move to higher wavenumber region, while the peaks of N-H shift to the opposite direction. These movements reveal effective interactions between PPy and **CuSiW$_{12}$**, which can be ascribed to the existence of hydrogen bonds and π-π interactions.[19]

Optical property

The UV-vis diffuse reflectance spectra (DRS) of **CuSiW$_{12}$** and **PPy/CuSiW$_{12}$** composite materials were studied. Compared with visible light inactive **CuSiW$_{12}$**,

PPy/CuSiW$_{12}$ composite materials show strong absorptions in ultraviolet and visible light region, which suggests PPy is a suitable option to extend the photoresponse region of **CuSiW$_{12}$** (Fig. 5a). To study the influences of temperature on photoresponse region, band gaps (E_g) of all the **PPy/CuSiW$_{12}$** composite materials were obtained from Tauc equation (Fig. 5b). We find E_g values of these composite materials increase with the enhancement of reaction temperature. In these **PPy/CuSiW$_{12}$** composite materials, **PPy(A)/CuSiW$_{12}$** possesses the narrowest band gap.

Electrochemical analysis

The interface charge separation efficiency can be investigated by photocurrent spectra, incident photon-to-electron conversion efficiency (IPCE) and electrochemical impedance spectroscopy (EIS). Photocurrent responses indicate in visible light region, photocurrent intensities of **PPy/CuSiW$_{12}$/ITO** electrodes are much stronger than **CuSiW$_{12}$/ITO** electrode, which indicates the loading of PPy on surface of **CuSiW$_{12}$** can enhance its photocurrent effectively. Furthermore, with the raising of reaction temperature, photocurrent intensity of **PPy/CuSiW$_{12}$/ITO** electrodes decrease and **PPy(A)/CuSiW$_{12}$/ITO** electrode exhibits the largest photocurrent intensity (Fig. 6a). As photocurrent spectra, after the loading of PPy, IPCE also enhances (Fig. 6b). The maximum IPCE value is also observed on **PPy(A)/CuSiW$_{12}$/ITO** electrode (14.22%), which is about 7.29 fold larger than that of **CuSiW$_{12}$/ITO** electrode (1.95%).

To study the charge separation and transfer process in detail, EIS was employed (Fig. 6c). In EIS, the radius of the *arc* on Nynquist plot reflects the reaction rate occurred on the surface of the electrode.[20] The *arc* radius of **PPy/CuSiW$_{12}$/ITO** electrodes are all smaller than **CuSiW$_{12}$/ITO** electrode, which illustrates a more effective separation of photogenerated electron-hole pair as well as a faster interfacial charge transfer have occurred after the loading of PPy. In the composite material

electrodes, **PPy(A)/CuSiW$_{12}$/ITO** electrode exhibits smallest *arc* radius, which implies it possesses the highest photogenerated charge separation efficiency.

In summary, the electrochemical tests are well matched with the optical property studies. All these results indicate the loading of PPy on surface of **CuSiW$_{12}$** decreases the recombination of photogenerated electron-hole pair. Furthermore, compared with high temperature, low temperature is a more appropriate condition to fabricate composite material with excellent electron-hole pair separation efficiency.

Photocatalytic property study

The photocatalytic activities of **CuSiW$_{12}$** and **PPy/CuSiW$_{12}$** composite materials were evaluated by the degradation of RhB in aqueous solution (Fig. 7). Like other SiW$_{12}$ based photocatalysts, as an ultraviolet light active photocatalyst, **CuSiW$_{12}$** exhibits no effect on RhB in visible light region, but its composite materials show more excellent photocatalytic activities in visible light region (Fig. S2). Furthermore, we can find with the increasing of temperature their photocatalytic activities decrease monotonously (Fig. 8a). This can be also attributed to the difference in conductivity of PPy loading on **CuSiW$_{12}$** (Fig. 8b). At low temperature, during polymerization process, the PPy particles grow slowly. PPy obtained under this condition arrange trimly and exhibit high conductivity. But as temperature raises, the growth of PPy become quickly and the defects in PPy chains also increase, which will destroy π-conjugated structure of PPy and decrease their conductivity. So, in these composite materials, **PPy(A)/CuSiW$_{12}$** exhibits highest photocatalytic efficiency. This is in accordance with the optical and electrochemical studies. To our interests, all the UV curves show blue-shift during decomposition process of RhB. This can be attributed to the missing of ethyl groups from RhB.[21] To illustrate this imagination, the degradation products are studied by HPLC-MS (Fig. S3). From these results, we can

conclude, during the photocatalytic process, N, N-diethyl-N'-ethylorhodamine, N-diethyl-N'-ethylorhodamine, N, N'-diethylrhodamine, N-ethylrhodamine and rhodamine are produced successively. The final product of this decomposition process is rhodamine.

In photocatalytic degradation reaction, the activity and stability of recycled catalyst are very important factors to determine the performance of a photocatalyst. Herein, photocatalytic property of **PPy(A)/CuSiW$_{12}$** are re-examined for five times and the recycled photocatalysts still show excellent photocatalytic properties (Fig. 8c). Furthermore, the recycled sample also exhibits similar PXRD patterns with original composite material, which indicates the structure of **PPy(A)/CuSiW$_{12}$** is not destroyed during the photocatalysis decomposition process of RhB (Fig. 8d).

Mechanism study

For PPy based composite material, the enhancement of photocatalytic activity originates from the synergy between PPy and the other component. To illustrate this point clearly, PPy and **PPy/CuSiW$_{12}$M** (mechanically blended product of PPy and **CuSiW$_{12}$M**) were used as reference to evaluate the photocatalytic efficiency (Fig. 9a, 9b and Fig. S4, S5). Furthermore, the photocatalytic efficiency of $Cu(NO_3)_2 \cdot 3H_2O$, bpca, pca and $H_4SiW_{12}O_{40}$ were also investigated (Fig S6). It is notable their photocatalytic properties are much weaker than **PPy/CuSiW$_{12}$** composite materials. This implies the synergy between PPy and **CuSiW$_{12}$** plays a crucial role in the improvement of photocatalytic activity.

During photocatalytic process, the detection of main oxidant is also very important, which can be carried out through radical and hole trapping experiments by using Na_2EDTA (hole scavenger) and *t*BuOH (radical scavenger) respectively.[22,23] It can be observed the photodegradation process decelerates distinctively when Na_2EDTA is

added. Furthermore, the addition of *t*BuOH also leads to the suppression of photodegradation rate (Fig. 9c). These imply hole and radical play the same role in the decomposition of organic dye.

Based on experimental findings and observations, we speculate the mechanism of **PPy/CuSiW$_{12}$** as follows (Fig. 9d). For **CuSiW$_{12}$**, its valence band (VB) and conduction band (CB) match well with the lowest unoccupied molecular orbital (LUMO) and highest occupied molecular orbital (HOMO) of PPy. So, under visible light irradiation, PPy is excited and produces electrons on its LUMO orbital, and then the electrons transfer into the CB of **CuSiW$_{12}$**, at the same time, the holes are born on VB of **CuSiW$_{12}$** and inject to HOMO of PPy. This process leads to the charge separation and stabilization, which hinders the recombination of electrons and holes. The resulting electrons and holes can further yield super oxide radial O_2^- and hydroxyl radical ·OH, which possess capability to decompose RhB effectively. Based on aforementioned points, in **PPy/CuSiW$_{12}$** composite material, the role of PPy can be described as efficient electron donors and good hole transporters.

Conclusions

With the in-situ chemical polymerization of Py, PPy were loaded on a new **TMCP/POM** successfully. We also discussed the influence of temperature on morphology, wettability, conductivity and photocatalytic activity. The optical condition to fabricate **PPy/CuSiW$_{12}$** composite material had been obtained. As expected, compared with **CuSiW$_{12}$**, PPy and their mechanically blended product, **PPy/CuSiW$_{12}$** composite materials exhibit much higher photocatalytic efficiency under irradiation of visible light. It can be concluded the fabrication of PPy loaded **TMCP/POM** composite material enable us to establish a feasible approach to improve photocatalytic property of **TMCP/POM**. Furthermore, PPy loaded

TMCP/POM composite material is a new kind of efficient photocatalyst for decontaminating colored wastewater produced in textile industries production.

Acknowledgements

This work was supported by National Natural Science Foundation of China (21303010, 21273029 and 21103017); Research Foundation for the Doctoral Program of Higher Education of China (20120042110024); Fundamental Research Funds for the Central Universities (N120405005); China Postdoctoral Science Foundation (201104568).

Electronic supplementary information (ESI) available: Crystal data and structure refinement results for **$CuSiW_{12}$**. TG curve of **$CuSiW_{12}$**. HPLC-MS of the degradation products during decomposition of RhB. Absorption spectra of RhB degraded with **$CuSiW_{12}$** under irradiation of ultraviolet light; Absorption spectra of RhB degraded with PPy and **PPy/$CuSiW_{12}$M** under irradiation of visible light. Absorption spectra of RhB degraded by $Cu(NO_3)_2 \cdot 3H_2O$; bpca; pca and $H_4SiW_{12}O_{40}$ under visible light irradiation.

Reference

1 (a) R. Asahi, T. Morikawa, T. Ohwaki, K. Aoki and Y. Taga, *Science* 2001, **293**, 269; (b) W. Zhao, W. H. Ma, C. C. Chen, J. C. Zhao and Z. G. Shuai, *J. Am. Chem. Soc*. 2004, **126**, 4782; (c) Y. Cong, J. L. Zhang, F. Chen and M. Anpo, *J. Phys. Chem. C* 2007, **111**, 6976.

2 (a) S. Kohtani, M. Koshiko, A. Kudo, K. Tokumura, Y. Ishigaki, A. Toriba, K. Hayakawa and R. Nakagaki, *Appl. Catal., B* 2003, **46**, 573; (b) S. Kohtani, M. Tomohiro, K. Tokumura and R. Nakagaki, *Appl. Catal., B* 2005, **58**, 265.

3 (a) C. H. Kim, B. H. Kim and K. S. Yang, *Carbon* 2012, **50**, 2472; (b) Z. Yang, S. Y. Gao, H. F. Li and R. Cao, *J. Colloid Interface Sci*. 2012, **375**, 172; (c) A. A. Ismail, *Appl. Catal., B* 2012, **117**, 67; (d) S. Civis, M. Ferus, M. Zukalova, P. Kubat and L. Kavan, *J. Phys. Chem. C* 2012, **116**, 11200.

4 (a) J. X. Meng, Y. G. Li, H. Fu, X. L. Wang and E. B. Wang, *CrystEngComm*. 2011, **13**, 649; (b) K. Wang, D. D. Zhang, J. C. Ma, P. T. Ma, J. Y. Niu and J. P. Wang, *CrystEngComm*. 2012, **14**, 3205; (c) W. Q. Kan, J. Yang, Y. Y. Liu and J. F. Ma, *Dalton Trans*. 2012, **41**, 11062. (d) Y. Q. Chen, S. J. Liu, Y. W. Li, G. R. Li, K. H. He, Y. K. Qu, T. L. Hu, X. H. Bu, *Cryst. Growth Des*. 2012, **12**, 5426.

5 (a) J. X. Meng, Y. Lu, Y. G. Li, H. Fu, X. L. Wang and E. B. Wang, *CrystEngComm*. 2011, **13**, 2479; (b) Y. Ding, J. X. Meng, W. L. Chen and E. B. Wang, *CrystEngComm*. 2011, **13**, 2687; (c) X. L. Wang, Y. F. Wang, G. C. Liu, A. X. Tian, J. W. Zhang and H. Y. Lin, *Dalton Trans*. 2011, **40**, 9299; (d) G. C. Liu, Y. F. Wang, A. X. Tian, X. L. Wang, J. J. Gao, S. Yang, H. Y. Lin, *Z. Anorg. Allg. Chem*. 2013, **639**, 148. (e) X. L. Wang, Q. Gao, A. X. Tian, G. C. Liu, *Cryst. Growth Des*. 2012, **12**, 2346;

6 (a) J. Y. Niu, S. W. Zhang, H. N. Chen, J. W. Zhao, P. T. Ma and J. P. Wang, *Cryst.*

Growth Des. 2011, **11**, 3769; (b) B. F. Meng, W. S. You, X. F. Sun, F. Zhang and M. Y. Liu, *Inorg. Chem. Commun*. 2011, **14**, 35; (c) Y. Q. Jiao, C. Qin, C. Y. Sun, K. Z. Shao, P. J. Liu, P. Huang, K. Zhou and Z. M. Su, *Inorg. Chem. Commun*. 2012, **20**, 273. (d) X. L. Wang, C. Xu, H. Y. Lin, G. C. Liu, J. Luan, Z. H. Chang, *RSC Advances*, 2013, **3**, 3592; (e) X. L. Wang, D, Zhao, A. X. Tian, J. Yin, *Dalton Trans*. 2014, **43**, 5211.

7 (a) H. X. Yang, T. F. Liu, M. N. Cao, H. F. Li, S. Y. Gao and R. Cao, *Chem. Commun*. 2010, **46**, 2429; (b) S. J. Li, S. M. Liu, S. X. Liu, Y. W. Liu, Q. Tang, Z. Shi, S. X. Ouyang and J. H. Ye, *J. Am. Chem. Soc*. 2012, **134**, 19716; (c) P. Huang, C. Qin, Z. M. Su, Y. Xing, X. L. Wang, K. Z. Shao, Y. Q. Lan and E. B. Wang, *J. Am. Chem. Soc*. 2012, **134**, 14004; (d) Y. H. Guo and C. W. Hu, *J. Mol. Catal. A: Chem*. 2007, **262**, 136.

8 (a) K. Murakoshi, R. Kogure, Y. Wada and S. Yanagida, *Sol. Energy Mater. Sol. Cells* 1998, **55**, 113; (b) R. Cervini, Y. Cheng and G. Simon, *J. Phys. D: Appl. Phys*. 2004, **37**, 13; (c) T. Kitamura, M. Maitani, M. Matsuda, Y. Wada and S. Yanagida, *Chem. Lett*. 2001, **10**, 1054.

9 (a) D. Chowdhury, A. Paul and A. Chattopadhyay, *Langmuir* 2005, **21**, 4123; (b) Q. L. Li, C. R. Zhang and J. Q. Li, *J. Alloys. Compd*. 2011, **509**, 1953; (c) D. Wang, Y. Wang, X. Li, Q. Luo, J. An and H. Yue, *Catal. Commun*. 2008, **9**, 1162.

10 (a) B. Wang, C. Li, J. F. Pang, X. T. Qing, J. P. Zhai and Q. Li, *Appl. Surf. Sci*. 2012, **258**, 9989; (b) S. N. Gu, B. Li, C. J. Zhao, Y. L. Xu, X. Z. Qian and G. R. Chen, *J. Alloys. Compd*. 2011, **509**, 5677; (c) X. C. Li, G. L. Jiang, G. H. He, W. J. Zheng, Y. Tan and W. Xiao, *Chem. Eng. J*. 2014, **236**, 480.

11 (a) T. A. Kandiel, R. Dillert and D. W. Bahnemann, *Photochem. Photobiol*. 2009, **8**, 683; (b) F. Deng, L. J. Min, X. B. Luo, S. L. Wu and S. L. Luo, *Nanoscale*

2013, **5**, 8703; (c) N. M. Dimitrijevic, S. Tepavcevic, Y. Z. Liu, T. Rajh, S. C. Silver and D. M. Tiede, *J. Phys. Chem. C* 2013, **117**, 15540.

12 (a) G. K. R. Senadeera, T. Kitamura, Y. Wada and S. Yanagida, *J. Photochem. Photobiol. A: Chem*. 2006, **184**, 234; (b) G. K. R. Senadeera, T. Kitamura, Y. Wada and S. Yanagida, *J. Photochem. Photobiol. A: Chem*. 2004, **164**, 61; (c) X. F. Lu, Q. D. Zhao, X. C. Liu, D. J. Wang, W. J. Zhang, C. Wang and Y. Wei, *Macromol. Rapid Commun*. 2006, **27**, 430.

13 (a) H. Yuvaraj, M. H. Woo, E. J. Park, Y. T. Jeong and K. T. Lim, *Eur. Polym. J.* 2008, **44**, 637; (b) Q. Cheng, Y. He, V. Pavlinek, C. Li and P. Saha, *Synth. Met.* 2008, **158**, 953; (c) C. Xu, J. Sun and L. Gao, *J. Mater. Chem*. 2011, **21**, 11253.

14 (a) S. C. Wuang, K. G. Neoh, E. T. Kang, D. W. Pack and D. E. Leckband, *J. Mater. Chem*. 2007, **17**, 3354; (b) Z. Zhang, Q. Li, L. Yu, Z. Cui, L. Zhang and G. A. Bowmaker, *Macromolecules* 2011, **44**, 4610; (c) F. Deng and Y. X. Li, *Colloids Surf., A* 2012, **395**, 183.

15 (a) G. M. Sheldrick, SHELX-97, Program for Crystal Structure Refinement; University of Göttingen, Germany, 1997; (b) G. M. Sheldrick, SHELX-97, Program for Crystal structure Solution; University of Göttingen, Germany, 1997.

16 (a) C. H. Zhang, Y. G. Chen, Q. Tang and S. X. Liu, *Dalton Trans*. 2012, **41**, 9971; (b) J. Q. Sha, J. W. Sun, M. T. Li, C. Wang, G. M. Li, P. F. Yan and L. J. Sun, *Dalton Trans*. 2013, **42**, 1667; (c) X. L. Wang, Y. F. Wang, G. C. Liu, A. X. Tian, J. W. Zhang and H. Y. Lin, *Dalton Trans*. 2011, **40**, 9299; (d) H. J. Pang, C. J. Gómez-García, J. Peng, H. Y. Ma, C. J. Zhang and Q. Y. Wu, *Dalton Trans*. 2013, **42**, 16596.

17 (a) Z. Y. Shi, Z. Y. Zhang, J.Peng, X. Yu and X. Wang, *CrystEngComm.* 2013, **15**, 7199; (b) X. Wang, J. Peng, M. G. Liu, D. D. Wang, C. L. Meng, Y. Li and Z. Y.

Shi, *CrystEngComm.* 2012, **14**, 3220; (c) H. J. Pang, H. Y. Ma, J. Peng, C. J. Zhang, P. P. Zhang and Z. M. Su, *CrystEngComm.* 2011, **13**, 7079; (d) P. P. Zhang, J. Peng, H. J. Pang, J. Q. Sha, M. Zhu, D. D. Wang and M. G. Liu, *CrystEngComm.* 2011, **13**, 3282; (e) J. Q. Sha, J. W. Sun, C. Wang, G. M. Li, P. F. Yan, M. T. Li and M. Y. Liu, *CrystEngComm.* 2012, **14**, 5053.

18 (a) X. P. Zhou, D. Li, S. L. Zheng, X. J. Zhang and T. Wu, *Inorg. Chem*. 2006, **45**, 7119; (b) J. V. Folgado, E. Coronado, D. Beltrán-Porter, R. Burriel, A. Fuertes and C. Miravitlles, *J. Chem. Soc., Dalton Trans.* 1988*,* 3041; (c) A. Kamiyama, T. Noguchi, T. Kajiwara and T. Ito, *Inorg. Chem.* 2002, **41**, 507.

19 (a) S. X. Min, F. Wang, Y. Q. Han, *J. Mater Sci*., 2007, **42**, 9966; (b) J. H. Wei, Q. Zhang, Y. Liu, R. Xiong, C. X. Pang, J. Shi, *J. Nanopart. Res*., 2011, **15**, 3157; (c) S. De, A. Dey, S. K. De, *J. Phys. Chem. Solids*, 2007, **68**, 66; (d) L. X. Zhang, P. Liu, Z. X. Su, *Polym. Degrad. Stab*., 2006, **91**, 2213.

20 (a) H. Liu, S. A. Cheng, M. Wu, H. J. Wu, J. Q. Zhang, W. Z. Li and C. N. Cao, *J. Phys. Chem. A* 2000, **104**, 7016; (b) W. H. Leng, Z. Zhang, J. Q. Zhang and C. N. Cao, *J. Phys. Chem. B* 2005, **109**, 15008.

21 T. watanabe, T. T akizava, K. Honda. *J. Phys. Chem*. 1977, **52**, 1845.

22 (a) T. Xu, Y. Cai and K. E. O'Shea, *Environ. Sci. Technol*. 2007, **41**, 5471; (b) H. Zhang, R. L. Zong and Y. F. Zhu, *J. Phys. Chem. C* 2009, **113**, 4605.

23 (a) Y. Lu, H. Yu, S. Chen, X. Quan and H. Zhao, *Environ. Sci. Technol*. 2012, **46**, 1724; (b) Y. Lin, D. Li, J. Hu, G. Xiao, J. Wang, W. Li and X. Fu, *J. Phys. Chem. C* 2012, **116**, 5764 (c) C. Minero, G. Mariella, V. Maurino, D. Vione and E. Pelizzetti, *Langmuir* 2000, **16**, 8964.

Table 1 Degradation efficiency of RhB with different photocatalysts

Photocatalyst	Condition	Time (hours)	η (%)
$CuSiW_{12}$	ultraviolet light irradiation	6	60.26
$CuSiW_{12}$	visible light irradiation	6	3.50
PPy(A)/$CuSiW_{12}$	visible light irradiation	2	85.92
PPy(B)/$CuSiW_{12}$	visible light irradiation	4	84.76
PPy(C)/$CuSiW_{12}$	visible light irradiation	4	72.32
PPy(A)	visible light irradiation	6	54.22
PPy (B)	visible light irradiation	6	43.65
PPy (C)	visible light irradiation	6	33.56
PPy(A)/$CuSiW_{12}$M	visible light irradiation	6	55.94
PPy(B)/$CuSiW_{12}$M	visible light irradiation	6	39.06
PPy(C)/$CuSiW_{12}$M	visible light irradiation	6	25.03

Figure Captions

Figure 1 (a) The fundamental unit of **$CuSiW_{12}$**; (b) **TMCP** in **$CuSiW_{12}$**; (c) 2D framework of **$CuSiW_{12}$**; (d) The "one stone two birds" hydrolysis process of tpt.

Figure 2 (a) SEM picture of **$CuSiW_{12}$**; (b) SEM picture **PPy(A)/$CuSiW_{12}$**; (c) SEM picture **PPy(B)/$CuSiW_{12}$**; (d) SEM picture **PPy(C)/$CuSiW_{12}$**.

Figure 3 The shape of a water droplet on the surface of (a) **$CuSiW_{12}$**; (b) **PPy(A)/$CuSiW_{12}$**; (c) **PPy(B)/$CuSiW_{12}$**; (d) **PPy(C)/$CuSiW_{12}$**.

Figure 4 (a) PXRD of **$CuSiW_{12}$** and **PPy/$CuSiW_{12}$**; (b) FTIR of **$CuSiW_{12}$** and **PPy/$CuSiW_{12}$**.

Figure 5 (a) DRS of **$CuSiW_{12}$** and **PPy/$CuSiW_{12}$**; (b) Tauc plots **$CuSiW_{12}$** and **PPy/$CuSiW_{12}$**.

Figure 6 (a) Photocurrent spectra of **$CuSiW_{12}$** and **PPy/$CuSiW_{12}$** under visible light; (b) IPCE of **$CuSiW_{12}$** and **PPy/$CuSiW_{12}$** electrodes under visible light; (c) EIS of **$CuSiW_{12}$** and **PPy/$CuSiW_{12}$** electrodes under visible light.

Figure 7 Absorption spectra of RhB degraded with different photocatalysts: (a) **$CuSiW_{12}$**; (b) **PPy(A)/$CuSiW_{12}$**; (c) **PPy(B)/$CuSiW_{12}$**; (d) **PPy(C)/$CuSiW_{12}$**.

Figure 8 (a) Degradation rate as the function of time by **$CuSiW_{12}$** and **PPy/$CuSiW_{12}$**; (b) Conductivities of **$CuSiW_{12}$** and PPy; (c) Cycling runs of the degradation of RhB in the presence of **PPy(A)/$CuSiW_{12}$**; (d) PXRD of recycled **PPy(A)/$CuSiW_{12}$**.

Figure 9 Degradation rate as the function of time (a) by **PPy**; (b) by **PPy/$CuSiW_{12}$M**; (c) Photocatalytic efficiency of **PPy/$CuSiW_{12}$** with existence of Na_2EDTA and BuOH. (d) Diagram of the photocatalytic mechanism for **PPy/$CuSiW_{12}$** under visible light.

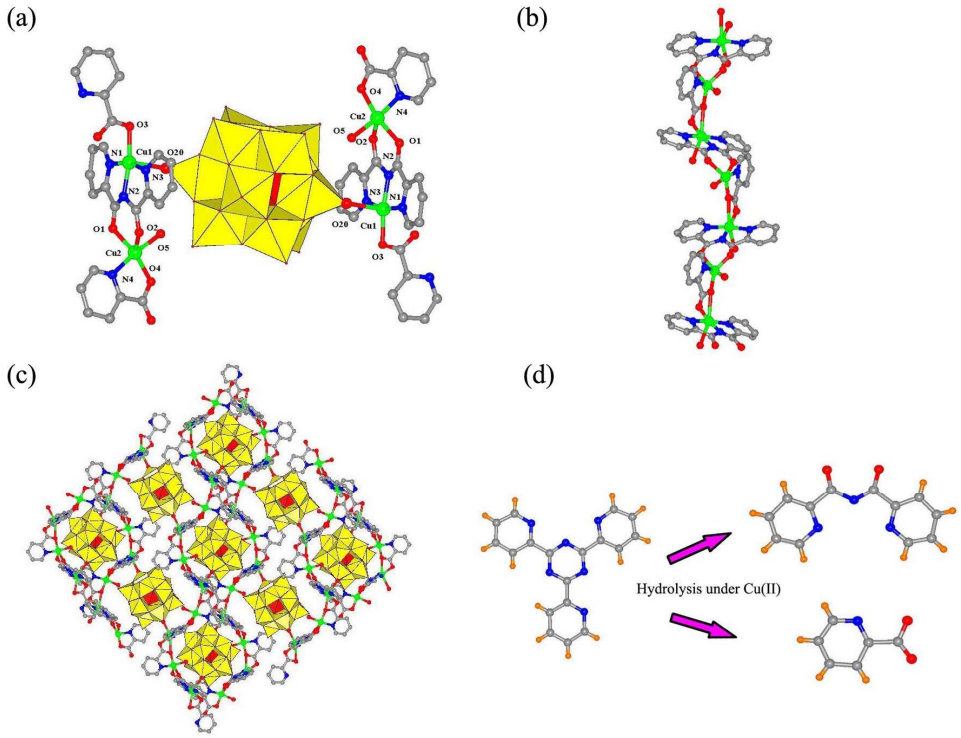

Figure 1

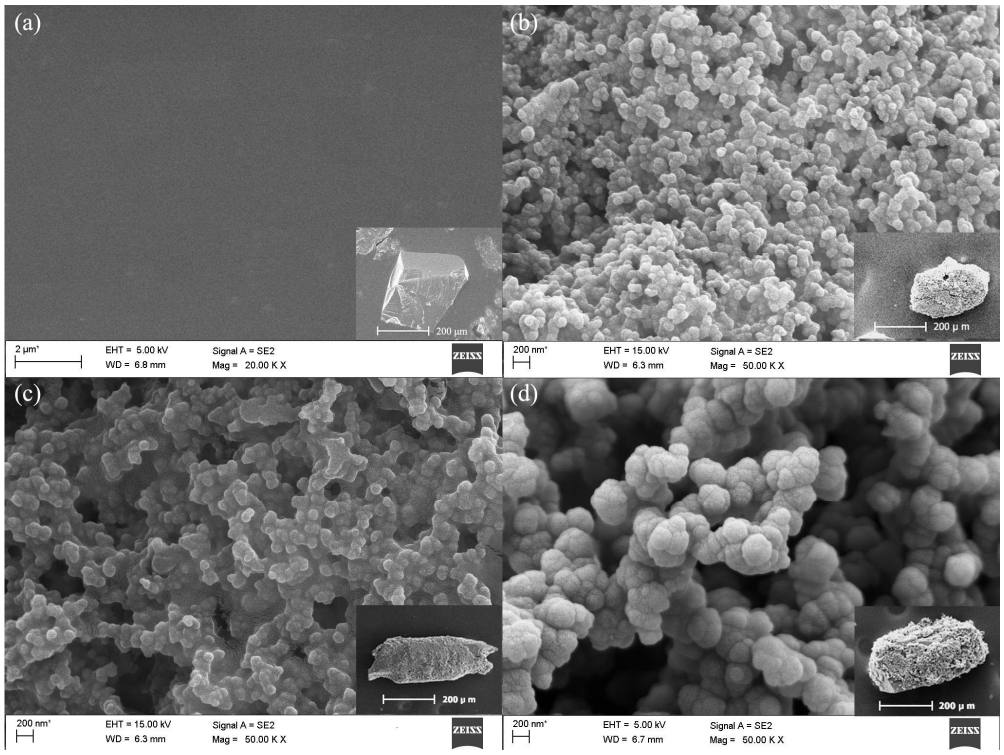
(a)
200 µm
2 µm*
EHT = 5.00 kV
WD = 6.8 mm
Signal A = SE2
Mag = 20.00 K X
ZEISS
(b)
200 µ m
200 nm*
EHT = 15.00 kV
WD = 6.3 mm
Signal A = SE2
Mag = 50.00 K X
ZEISS
(c)
200 µ m
200 nm*
EHT = 15.00 kV
WD = 6.3 mm
Signal A = SE2
Mag = 50.00 K X
ZEISS
(d)
200 µ m
200 nm*
EHT = 5.00 kV
WD = 6.7 mm
Signal A = SE2
Mag = 50.00 K X
ZEISS

Figure 2

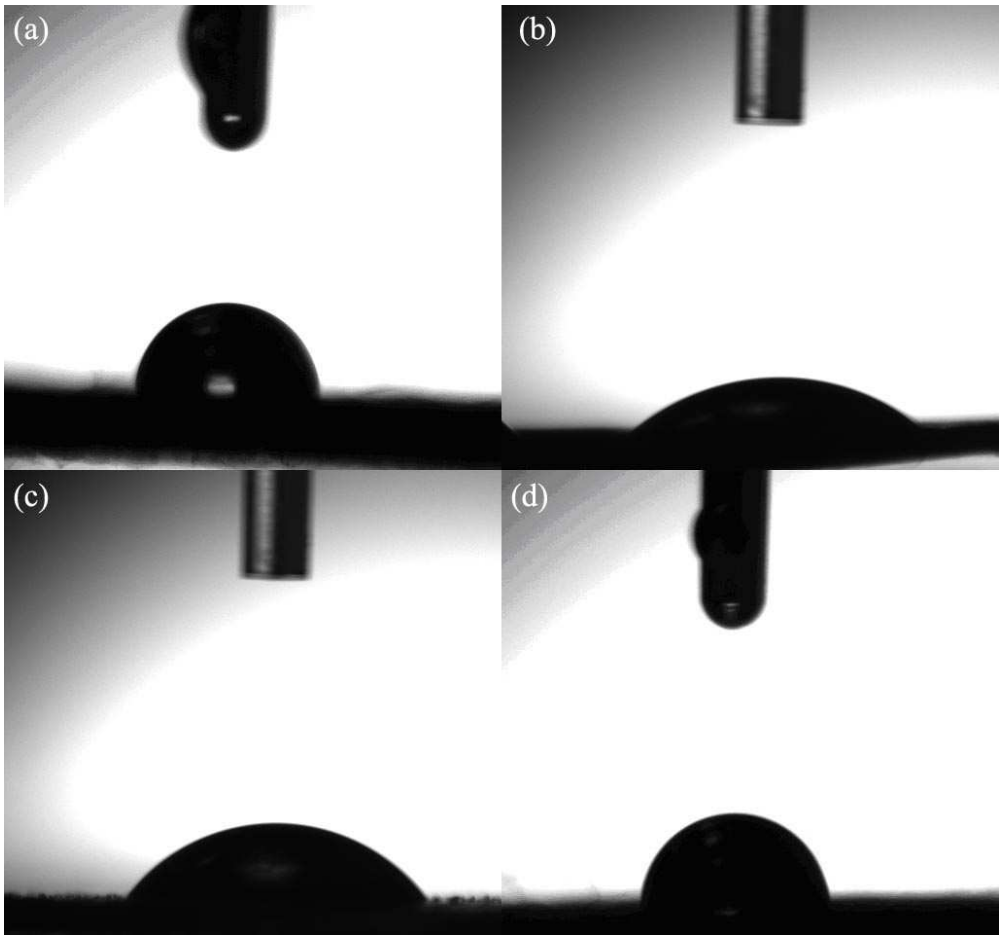

Figure 3

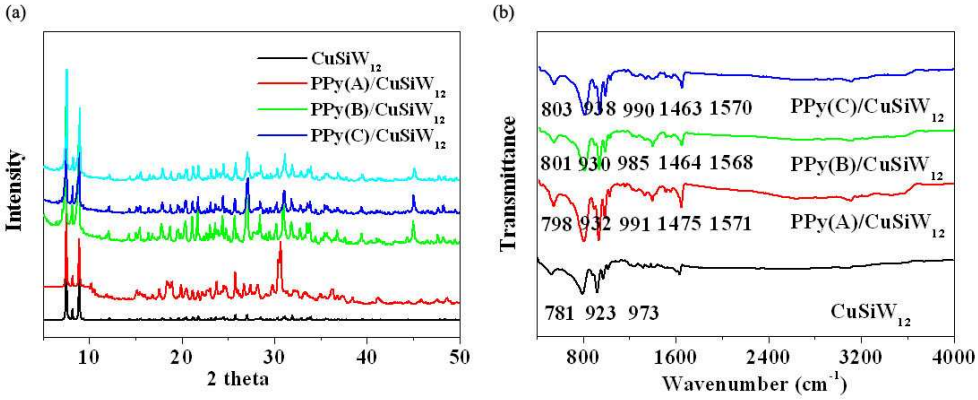
(a)
CuSiW12
PPy(A)/CuSiW12
PPy(B)/CuSiW12
PPy(C)/CuSiW12
Intensity
10
20
30
40
50
2 theta
(b)
803 938 990 1463 1570
PPy(C)/CuSiW12
801 930 985 1464 1568
PPy(B)/CuSiW12
798 932 991 1475 1571
PPy(A)/CuSiW12
781 923 973
CuSiW12
Transmittance
800
1600
2400
3200
4000
Wavenumber (cm-1)

Figure 4

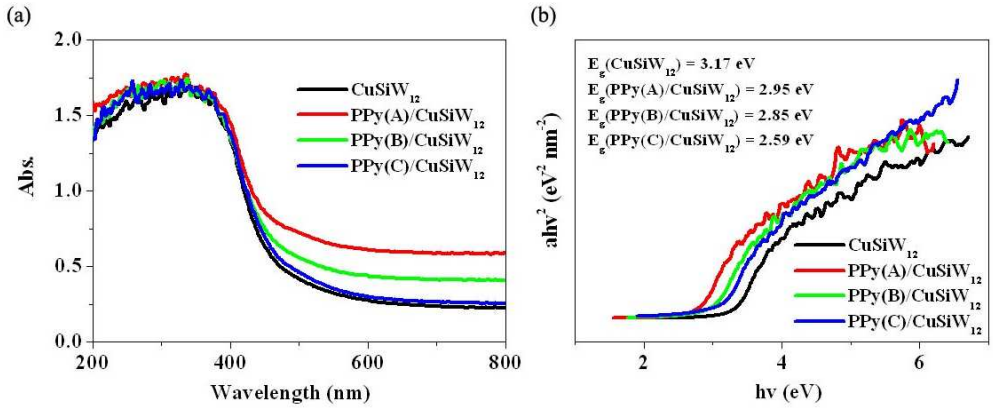
(a)
Abs.
Wavelength (nm)
CuSiW12
PPy(A)/CuSiW12
PPy(B)/CuSiW12
PPy(C)/CuSiW12
(b)
Eg(CuSiW12) = 3.17 eV
Eg(PPy(A)/CuSiW12) = 2.95 eV
Eg(PPy(B)/CuSiW12) = 2.85 eV
Eg(PPy(C)/CuSiW12) = 2.59 eV
αhν2 (eV-2 nm-2)
hν (eV)

Figure 5

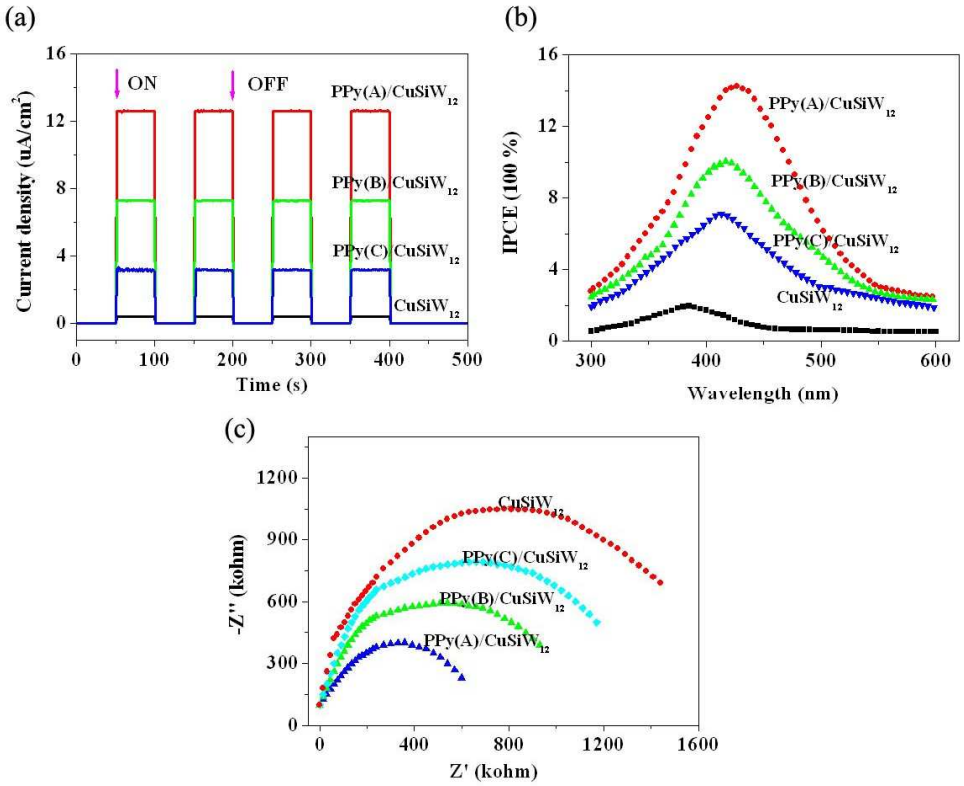
(a)
ON
OFF
PPy(A)/CuSiW12
PPy(B)/CuSiW12
PPy(C)/CuSiW12
CuSiW12
Current density (uA/cm2)
Time (s)
(b)
PPy(A)/CuSiW12
PPy(B)/CuSiW12
PPy(C)/CuSiW12
CuSiW12
IPCE (100 %)
Wavelength (nm)
(c)
CuSiW12
PPy(C)/CuSiW12
PPy(B)/CuSiW12
PPy(A)/CuSiW12
-Z'' (kohm)
Z' (kohm)

Figure 6

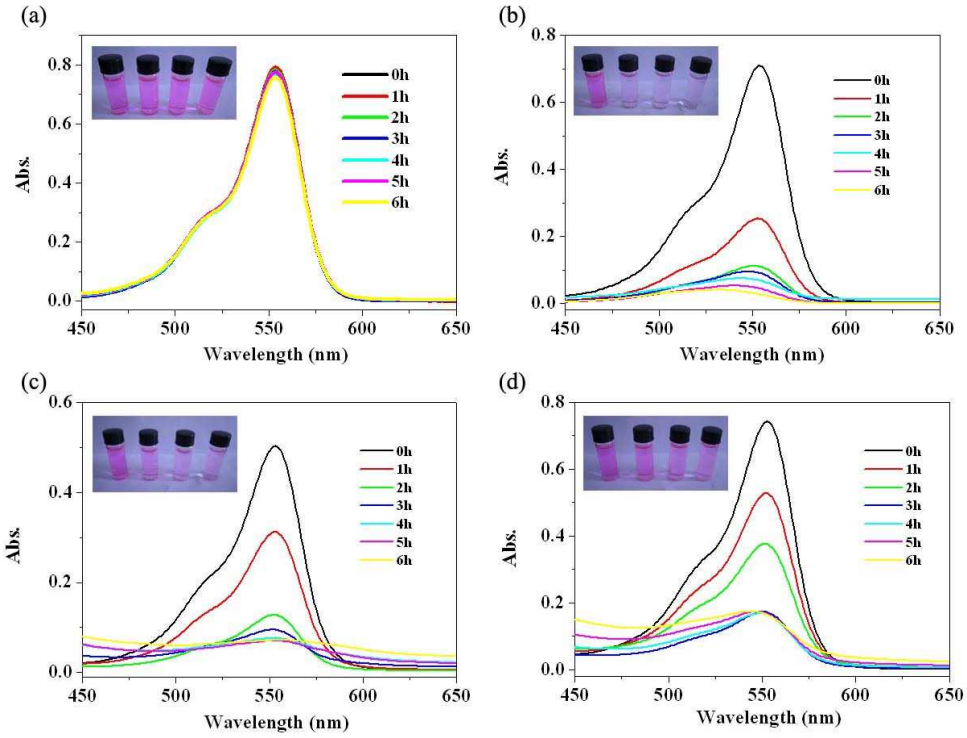

Figure 7

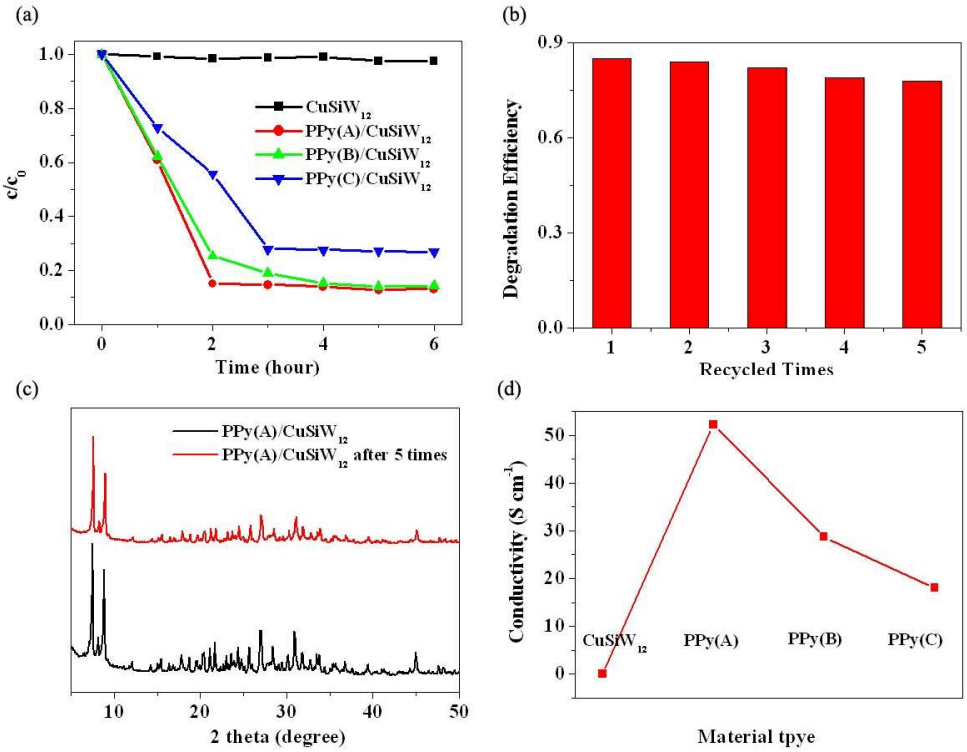
(a)
c/c0
Time (hour)
CuSiW12
PPy(A)/CuSiW12
PPy(B)/CuSiW12
PPy(C)/CuSiW12
(b)
Degradation Efficiency
Recycled Times
(c)
PPy(A)/CuSiW12
PPy(A)/CuSiW12 after 5 times
2 theta (degree)
(d)
Conductivity (S cm-1)
CuSiW12
PPy(A)
PPy(B)
PPy(C)
Material tpye

Figure 8

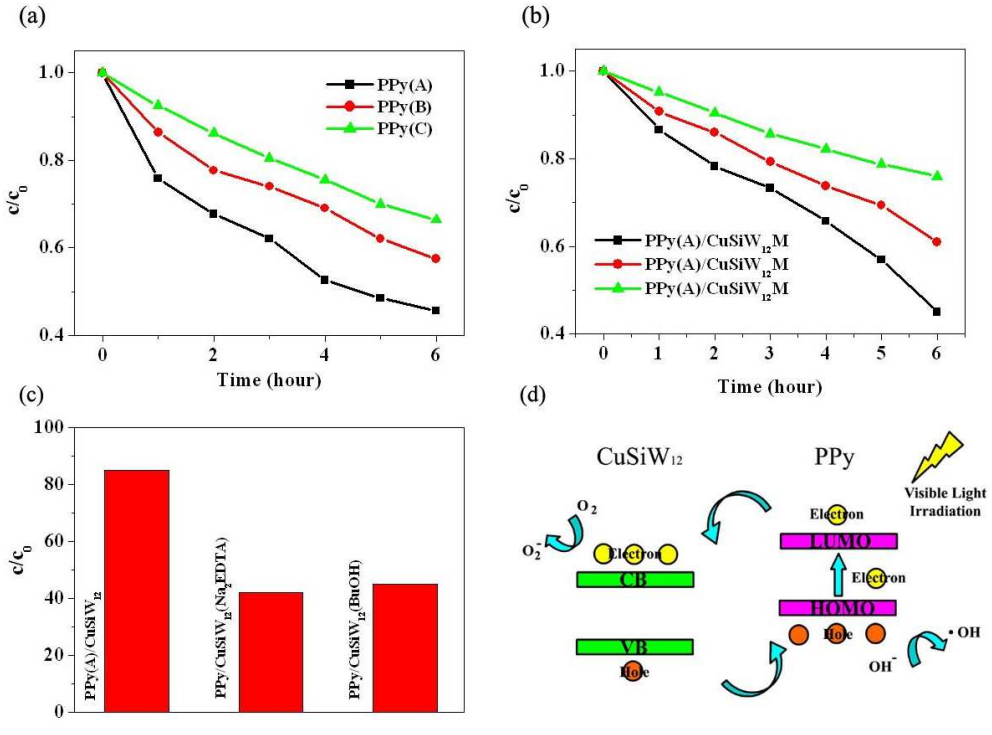
(a)
PPy(A)
PPy(B)
PPy(C)
c/c0
Time (hour)
(b)
PPy(A)/CuSiW12M
PPy(A)/CuSiW12M
PPy(A)/CuSiW12M
c/c0
Time (hour)
(c)
c/c0
PPy(A)/CuSiW12
PPy/CuSiW12(Na2EDTA)
PPy/CuSiW12(BuOH)
(d)
CuSiW12
PPy
Visible Light Irradiation
O2
O2-
Electron
CB
VB
Hole
Electron
LUMO
Electron
HOMO
Hole
OH-
• OH

Figure 9